The International Journal of Advanced Manufacturing Technology (2018) 97:1649–1661
https://doi.org/10.1007/s00170-018-1993-y

ORIGINAL ARTICLE

Comparative investigation on grindability of K4125 and Inconel718 nickel-based superalloys

Ning Qian[1] · Wenfeng Ding[1] · Yejun Zhu[1]

Received: 10 November 2017 / Accepted: 3 April 2018 / Published online: 30 April 2018

Abstract
Nickel-based superalloy is a typical hard-to-machining material in the aero-engine manufacturing industry. The grindability difference of two kinds of nickel-based superalloys, i.e., equiaxed cast nickel-based superalloy K4125 and wrought nickel-based superalloy Inconel718, are discussed in this article. The influence of grinding parameters (e.g., grinding speed, workpiece speed, and depth of cut) on the grinding force, grinding temperature, and ground surface quality are explored. The results illustrate that under the given grinding conditions, grinding K4125 generates higher forces than Inconel718. The temperature from the K4125 grinding process is beyond 400 °C, while the temperature from grinding on Inconel718 is below 200 °C. Moreover, because of the chip adhesion on the wheel surface when grinding K4125, not only the wheel wear is more severe but also the ground surface of K4125 is worse than that of Inconel718. Accordingly, it could be inferred that the grindability of K4125 is worse than that of Inconel718.

Keywords Nickel-based superalloy · K4125 · Inconel718 · Grindability · Ground surface

1 Introduction

Nickel-based superalloy is a kind of metallic material based on adding Co, Mo, Al, Nb, W, B, Ti, and other strengthening elements into the nickel-chromium matrix to ensure good thermal stability, thermal ductility, and corrosion resistance [1, 2]. For this reason, the nickel-based superalloy becomes the ideal material for parts used in combustors and turbines. Along with the development of aero-engines, the temperature of combustor exit and high-pressure turbine (HPT) always get higher and higher; the working temperature of the wrought nickel-based superalloys (e.g., Inconel718) no longer meets the requirement. Thereby, the cast nickel-based superalloy, which can sustain a higher temperature, is further invented.

On the other hand, those excellent properties of nickel-based superalloys also lead to difficulty in mechanical machining. In the common cutting process, the cutting force is usually large and the cutting temperature is also high. Furthermore, the tool wear is severe and the machining quality is unstable [3–6]. Under such conditions, the cutting technology could not meet the requirements in the present days, while grinding technology becomes an important method to machine nickel-based superalloy [7]. For this reason, it is necessary to investigate the grindability of the equiaxed cast nickel-based superalloy K4125 and provide the theoretical support for the industry.

As indicated in the previous literature, Xi et al. [8] researched the grindability difference among Inconel718 superalloy, Ti_2AlNb intermetallics, and Ti-6Al-4V alloy. The grinding forces and G-ratio during grinding Inconel718 superalloy are significantly higher than those during grinding Ti-6Al-4V alloy and Ti_2AlNb intermetallics; moreover, the ground surface quality of the Inconel718 is worse. Accordingly, it was inferred that Inconel718 superalloy was more difficult to grind than Ti-6Al-4V alloy and Ti_2AlNb intermetallics. Additionally, for a better understanding of material removal mechanism, Österle and Li [9] investigated the mechanical and thermal response of the IN738LC superalloy in grinding process with a high material removal rate, in which they looked into the alloy strength and contact temperature under some typical machining conditions. The temperature model was also established when grinding IN738LC with corundum wheel. According to the microstructure of ground surface, it was found that the temperature can reach to the melting point of the superalloy at the grain-workpiece contact point;

✉ Wenfeng Ding
dingwf2000@vip.163.com

[1] College of Mechanical and Electrical Engineering, Nanjing University of Aeronautics and Astronautics, Nanjing 210016, People's Republic of China

therefore, the white layer can be thick, and the surface condition was poor. However, the tensile residual stress and micro-cracks can be restricted under 10 μm thick by applying efficient coolant. Öpöz and Chen [10] used CBN grain scratch experiments to detect the material removal mechanism, side-flow and pile-up phenomenon during the grinding process of the Inconel718 superalloy. In the process, quantities and shapes of the cutting edges changed when the grains wore out; hence, the machinability of the CBN grains would be descent and the pile-up ratio of the ground surface would increase. Additionally, Tian et al. [11] investigated the influence of grinding speed on the material removal mechanism of Inconel718 through the twice single grain scratch experiments. In his research, the size effect and speed effect were proposed. Dai et al. [12] analyzed the chip formation and grinding forces in single grain grinding of Inconel718 by means of the finite element simulation. It was found that the grinding speed generally has a major influence on the chip formation. However, when the undeformed chip thickness is fixed, the grinding speed hardly affects average grinding forces. Dai et al. [13] conducted single grain grinding experiments of Inconel718 to analyze the effect of grain wear on the material removal behavior. The grain wear was usually in the form of crater wear, flank wear, micro-fracture, and macro-fracture. When the grain wear occurred, the rake angle of the cutting edge increased; then, the force ratio rose and the machinability decreased. Furthermore, in order to achieve a better grinding performance, Liu et al. [14] comparatively assessed the corundum wheels and superabrasive wheels in grinding Inconel718 via performance-cost analysis. Chen et al. [15] and Li et al. [16] developed porous and brazed CBN wheels to grind Inconel718 superalloy; the burn-free and quality stable surfaces were achieved. Additionally, Zhong et al. [17] researched the ultra-high-speed grinding of Inconel718, which decreased grinding force and residual stress and improved the surface quality. Generally, the superabrasive wheels performed better than the corundum wheels in surface grinding; however, the superabrasive wheels usually have a higher cost and especially are difficult to dress in profile grinding process.

Because the cast nickel-based superalloy has the excellent thermal strength and low heat conductivity, it is harder to machine than the wrought nickel-based superalloy. Due to the difficulty, several researchers explored the process strategy of grinding the cast nickel-based superalloy. For example, Xu et al. [18] analyzed the influence of grinding temperature on the surface integrity when grinding K417. They drew the conclusion that grinding temperature had a major impact on the surface roughness, though no crack was caused. Accordingly, the grinding process may be divided into two steps: the first step was to enhance the material removal rates without concerning about the surface burn because the heat-affected zone was only 40 μm thick. The second step was to clean the heat-affected layer by a small depth of cut to meet the requirement. Furthermore, Ding et al. [19, 20] researched the grindability, surface integrity, and tool wear when creep-feed deep grinding K424 cast superalloy with a brazed CBN wheel. Relied on the good heat conductivity, efficient storage space, and high protrusion height of the wheel, the straight groove was successfully ground and the grinding temperature was controlled below 100 °C. They also discovered that grinding temperature was a vital cause of the grain wear, which could be classified into mild wear (e.g., attrition wear and micro-fracture of the grain) and severe wear (e.g., macro-fracture of the grain and erosion of the bonding layer). It is noted that even though the material removal mechanism of grinding nickel-based superalloy has been explored by several scholars, and the grinding performance of some nickel-based superalloys has been investigated, the grindability of different superalloys is significantly different. Therefore, as a newly invented cast nickel-based superalloy, the grindability of K4125 superalloy is pending to explore. In addition, the Inconel718 superalloy is a typical hard-to-machining material. The grindability of K4125 can be clearly revealed by comparing with that of Inconel718. As a result, it is necessary to conduct the comparative investigation on the grindability of K4125 and Inconel718.

Though some researchers have pointed out that CBN wheel performs better when grinding nickel-based superalloy, the CBN wheel still encounters a great problem of dressing nowadays. Owing to the convenience of dressing and a lower cost, the corundum wheel is still widely applied in grinding of hard-to-machining alloys. For example, Tso [2] studied the grinding of Inconel718 via WA, GC, and CBN wheels. It is found that WA wheel performed better than GC wheel but worse than CBN wheel. However, the cost of WA wheel takes the advantage over the CBN wheel. Spur and Niewelt [21] ground the IN738LC and SC16 single crystal alloy via the corundum wheel. They found that the grinding force of IN738LC scattered around 60 N along with a severe wheel wear, while the grinding force of SC16 was 50% lower due to the material characteristics. Zhao et al. [22] ground the Inconel718 through two SG wheels and one PA wheel with a specific pore volume of 13.5, 14.4, and 13.4%, respectively. The wheel with a larger pore volume can decrease the grinding force, specific energy, and grinding temperature and improve the ground surface. Sinha et al. [23] conducted the comparative investigation on surface burn during dry grinding of Inconel718 with silicon carbide and alumina wheel. The burn-free surface was obtained through the alumina wheel, while the ground surface was easily burnt out by silicon carbide wheel because of the dissociation of SiC and severe diffusion of carbon over the ground surface.

Given all that, aimed at developing the strategy of grinding the equiaxed cast nickel-based superalloy

Table 1 Chemical composition of K4125 and Inconel718 Nickel-based superalloy

Element	Chemical composition/wt%	
	K4125	Inconel718
C	0.09–0.13	≤ 0.08
Cr	8.7–9.1	17.0–21.0
Co	9.5–10.5	≤ 1.0
W	6.6–7.4	–
Mo	1.6–2.4	2.80–3.30
Al	4.6–5.0	0.30–0.70
Ti	2.3–2.7	0.75–1.15
B	0.01–0.02	≤ 0.006
Zr	0.03–0.07	–
Ta	3.6–4.0	–
Hf	1.4–1.7	–
Nb	–	4.75–5.50
Mn	–	≤ 0.35
Si	–	≤ 0.35
Ni	Balance	50.0–55.0
Fe	–	Balance

K4125, this article concentrates on the grinding performance of K4125 by the brown corundum wheel. A comparative investigation is conducted on K4125 and Inconel718 to explore the influence of grinding parameters on the grinding force, specific grinding energy, grinding temperature, and machined surface quality.

2 Experimental materials and conditions

2.1 Workpiece materials

The workpiece materials used are equiaxed cast nickel-based superalloy K4125 and wrought nickel-based superalloy Inconel718. The chemical composition and mechanical property are listed in Table 1 and Table 2 [8]. According to Table 2, at a middle-temperature range, K4125 could bear a resemblance to the mechanical property of Inconel718; at a high-temperature range, however, the K4125 always has a better thermal strength and stability, creep and impact resistance than Inconel718.

Table 2 Mechanical property of K4125 and Inconel718 nickel-based superalloy

Property	K4125	Inconel718	K4125	Inconel718
Testing temperature/°C	650		1050	900
Tensile strength/MPa	830	900	480–499	140–280
Reduction of area/%	≥ 6.0	8.0	–	–

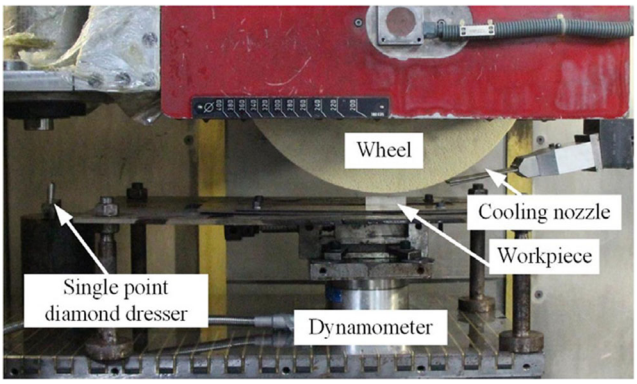

Fig. 1 Grinding experimental setup

2.2 Experimental setup

The setup of the grinding experiment is shown in Fig. 1. All tests were carried out on the Blohm Profimat MT-408 surface grinder, the maximum output power of which is 45 kW, and the maximum rotational speed is 8000 rpm. The grinding wheel is brown corundum wheel, coded as F13A80FF22V35M, as shown in Fig. 2. The grain is in 80 US mesh with a grain diameter of 160–200 μm. The porosity of the wheel is 23% and the hardness grade is F. The dimension of the workpiece is 25 mm long by 25 mm high and by 5 mm wide. The detailed grinding condition is listed in Table 3. After each grinding path, the corundum wheel was dressed by a single point diamond dresser. The dressing parameters: the dressing speed of $v_d = 20$ m/s, workpiece speed of $f_d = 200$ mm/min, and the depth of cut of $a_d = 0.01$ mm, were applied. Under such condition, nearly every grain on the wheel surface can be dressed [8]. The coolant used was the 5% emulsified water with 90 L/min flow capacity at 1.5 MPa pressure [24].

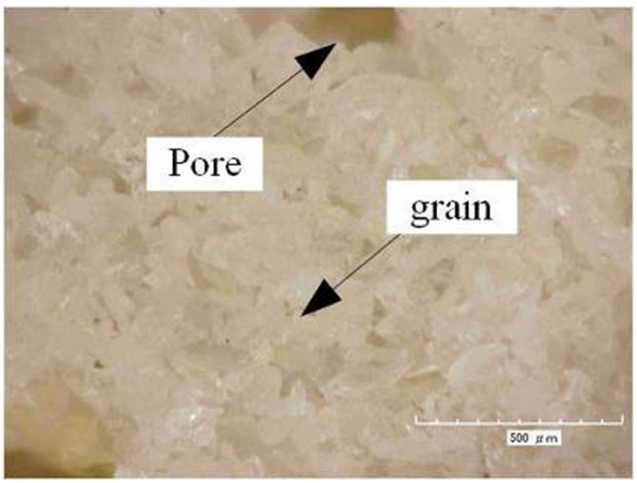

Fig. 2 Brown corundum wheel surface

Table 3 Grinding experimental conditions

Machine tool	Blohm Profimat MT-408 surface grinder
Grinding mode	Surface down-grinding
Abrasive wheel	Brown corundum wheel (80 US Mesh)
Wheel speed v_s/(m/s)	15–30
Workpiece speed v_w/(mm/min)	480–1800
Depth of cut a_p/(mm)	0.01–0.4
Grinding width b/(mm)	5
Cooling mode	5% emulsified water; 90 L/min, pressure at 1.5 MPa

2.3 Testing method

Aimed at exploring the grindability of K4125 and Inconel718, the horizontal and vertical force signals were captured by Kistler 9317C piezoelectric dynamometer and amplified by Kistler 5018A current amplifier. The signals were processed by DynoWare software to transfer to force values. The grinding zone temperature was measured by Constantan-workpiece semi-artificial thermocouple and NI USB6008 card [15, 19]. The spindle power was measured by Load Controls PPC-3 Power cell with the full scale of 100 kW. Every test was undertaken triple times to get reliable data.

The ground surface was observed by Sensofar S Neox 3D confocal microscopy and HK-7700 3D microscopy. The surface roughness R_a was measured by MAHR M2 perthometer. Meanwhile, the HK-7700 3D microscopy was applied to observe the wheel surface and count the active cutting points.

3 Experimental results and discussion

3.1 Grinding force and specific grinding energy analysis

Grinding force has a great influence on the grinding temperature, residual stresses, tool wear, etc. Therefore, it is necessary to investigate the grinding force for a better understanding of the grindability of K4125 and Inconel718 superalloys [25, 26].

Figure 3a illustrates that the normal and tangential grinding forces F_n, F_t rise with the increase of depth of cut a_p, which is due to a larger undeformed chip thickness a_{gmax} relatively. When the depth of cut increases from 0.01 to 0.1 mm, a_{gmax} rises from 0.38 to 0.68 μm, which are calculated by Eq. 1, and the tangential force of K4125 and Inconel718 increase from

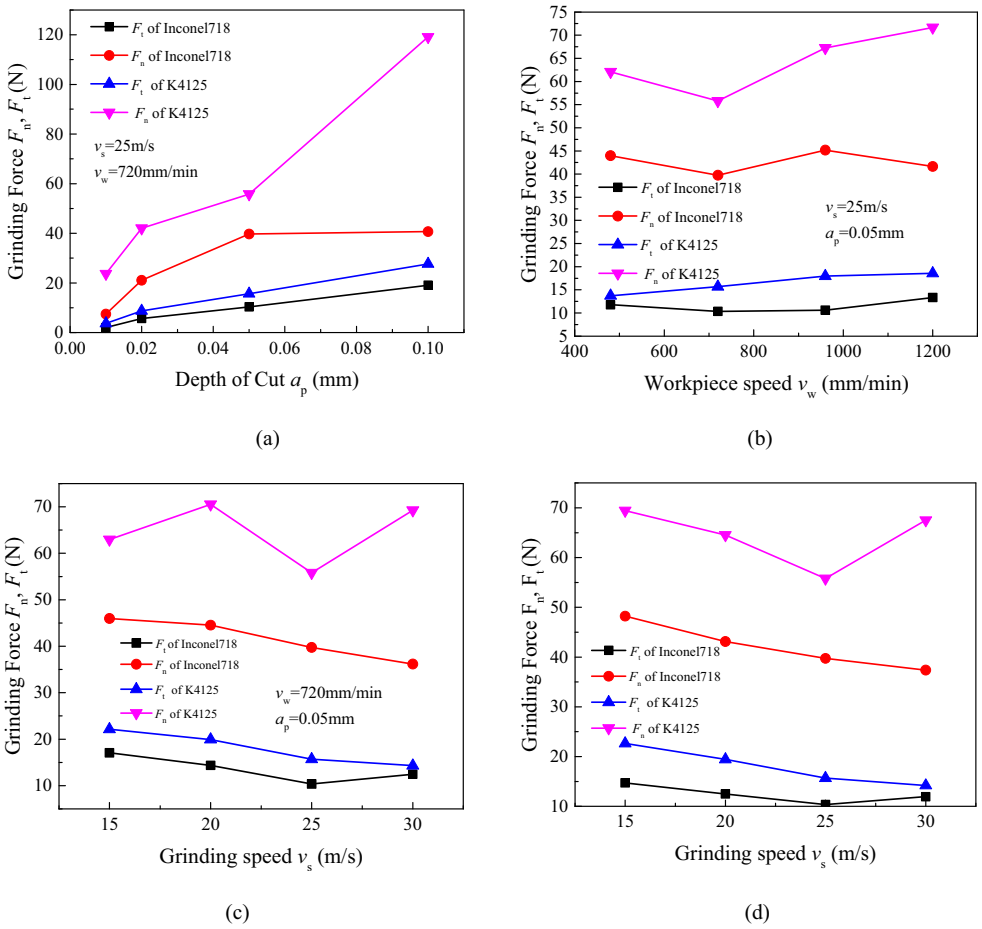

Fig. 3 Effects of **a** depth of cut, **b** workpiece speed, **c** grinding speed and **d** grinding speed with fixed undeformed chip thickness on grinding force components

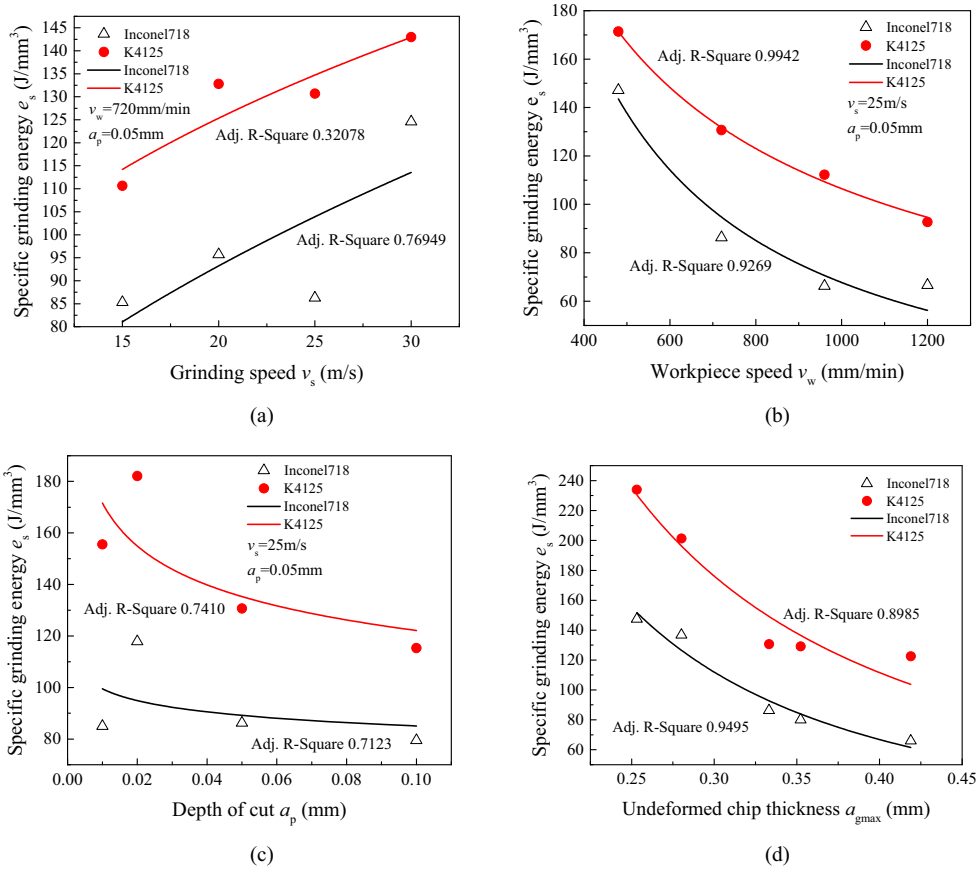

Fig. 4 Effects of **a** grinding speed, **b** workpiece speed, **c** depth of cut and **d** undeformed chip thickness on specific grinding energy

3.81 to 29.01 N and 2.22 to 19.34 N, respectively. The normal forces of K4125 and Inconel718 change at the same trend when the depth of cut is from 0.01 to 0.05 mm. However, when the depth of cut is above 0.05 mm, the normal force of K4125 sharply rises from 55.8 to 119.13 N by 113%, and the normal force of Inconel718 increases slightly from 39.74 to 40.67 N by 2.34%. It is illustrated in Fig. 3b that the tangential force of K4125 and Inconel718 show a similar changing tendency with the workpiece speed v_w rising from 480 to 1200 mm/min. Furthermore, the normal force of K4125 and Inconel718 scattered around 60 and 40 N as the workpiece speed increases from 480 to 960 mm/min. The normal forces increase slowly from 67.27 to 71.68 N for K4125 rather than decrease from 45.14 to 41.65 N for Inconel718, as workpiece speed changes from 960 to 1200 mm/min. The tangential force of K4125 and Inconel718 and normal force of Inconel718 generally decrease slightly as the grinding speed rises, which is due to the fact that a_{gmax} descents from 0.74 to 0.52 μm with the enhancement of

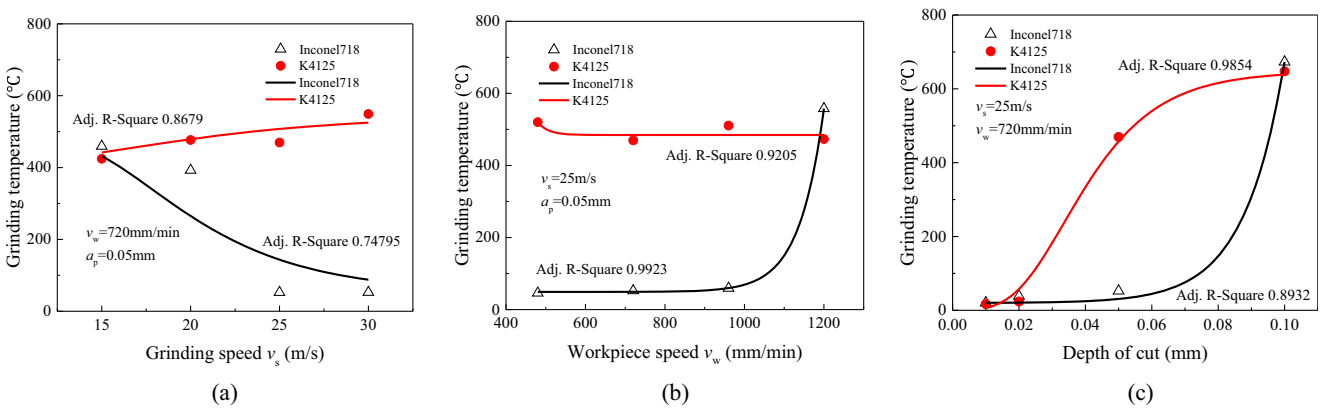

Fig. 5 Effects of **a** grinding speed, **b** workpiece speed and **c** depth of cut on the grinding temperature

Table 4 R_w of K4125 and Inconel718

	v_s (m/s)	v_w (mm/min)	a_p (mm)	F_t (N)	R_w (%)
K4125	15	720	0.05	22.13	0.251
	20	720	0.05	19.92	0.271
Inconel718	15	720	0.05	17.07	0.555
	20	720	0.05	14.36	0.488

the v_s from 15 to 30 m/s, leading to a smaller load on the abrasive wheel. At the same time, the normal force of K4125 scatters around 60 N since the grinding speed rises from 15 to 30 m/s, as demonstrated in Fig. 3c.

In particular, the undeformed chip thickness a_{gmax} in grinding is determined by the following expression:

$$a_{gmax} = \sqrt{\frac{4v_w}{v_s N_d C}\sqrt{\frac{a_p}{d_s}}} \tag{1}$$

where N_d is the active cutting point (i.e., 12 mm^{-2} as measured by the microscope in this experiment), C is a constant related with the shape of the grain, and for grain with 160–200 μm in diameter, it is taken to 6.89. d_s is the diameter of the wheel (i.e., 400 mm in this experiment).

Furthermore, when the grinding speed over workpiece speed (v_s/v_w) is fixed, that is a_{gmax} stays unchanged, increasing grinding speed brings about a higher thermal softening effect and a lower workpiece strength [12]. Thereby, the grinding force of K4125 and Inconel718 decreases accordingly when the grinding speed rises from 15 to 25 m/s, as shown in Fig. 3d. However, when the grinding speed is above 25 m/s, the normal force of K4125 increases slightly from 55.80 to 67.51 N, while the normal force of Inconel718 continues dropping. Besides, it is found in Fig. 3 that the grinding force of K4125 is always larger than that of Inconel718 by maximum 68.40%, under no matter what conditions.

Specific grinding energy e_s is another important index of grindability, which means the required energy to remove a unit volume of workpiece material. The expression is followed as:

$$e_s = \frac{P}{bv_w a_p} = \frac{F_t v_s}{bv_w a_p} \tag{2}$$

where P is the grinding power and b is the width of the grinding zone.

The specific grinding energy from grinding K4125 and Inconel718 enhances along with the increase of grinding speed, as illustrated in Fig. 4a, while the specific grinding energy descents along with the rise of the workpiece speed and depth of cut, as shown in Fig. 4b, c. This trend agrees well with the expression of specific grinding energy above. Figure 4d demonstrates the effect of undeformed chip thickness a_{gmax} on the specific grinding energy, which shows that the smaller the undeformed chip thickness is, the larger the specific energy is. This phenomenon can be explained by the size effect [14, 27–29]. Fitted by the least square method, the specific grinding energy is represented by the following expression:

$$\text{For K4125}: e_s = 26.11 a_{gmax}^{-1.59} \tag{3}$$

$$\text{For Inconel718}: e_s = 12.94 a_{gmax}^{-1.79} \tag{4}$$

In short, the recorded specific grinding energy of K4125 is in the range of 100–240 J/mm^3 in regardless of grinding parameters in the present experimental investigation. Nonetheless, the specific grinding energy of Inconel718 changes in the range of 60–150 J/mm^3. Therefore, it is clear that the specific grinding energy of K4125 is always higher than that of Inconel718, maximum by 45.40%.

3.2 Grinding temperature analysis

Grinding nickel-based superalloy always generate a lot of energy, and most of the energy (more than 90%) would transfer into the workpiece materials, abrasive wheel, and cooling fluid by the form of heat [30]. The grinding temperature usually reaches to 400 °C easily when grinding superalloys, which brings about thermal stress, cracks, surface burns, softening, residual stress, etc. [31, 32].

Figure 5 shows the effect of grinding parameters on the grinding temperature. When grinding K4125 at a speed of 15–25 m/s, the grinding temperature maintains an increasing trend above 400 °C, though the temperature generated by grinding Inconel718 decreases from 459.42 °C significantly to 52.82 °C, as shown in Fig. 5a. Figure 5b illustrates that the grinding temperature of K4125 remains stable above 500 °C along with the increase of workpiece speed; at the same time, the grinding temperature of Inconel718 slightly grows from 46.1 to 59.4 °C initially, then dramatically increases to 558 °C because of the

Table 5 The simulated temperature and thermal field depth of K4125 and Inconel718

Items	K4125				Inconel718			
Grinding speed (m/s)	15	20	25	30	15	20	25	30
Simulated temperature (°C)	420.23	482.33	459.62	552.82	422.35	372.05	80.56	85.47
Depth of thermal field (mm)	2.67	2.69	2.43	2.90	5.12	4.69	3.48	3.50

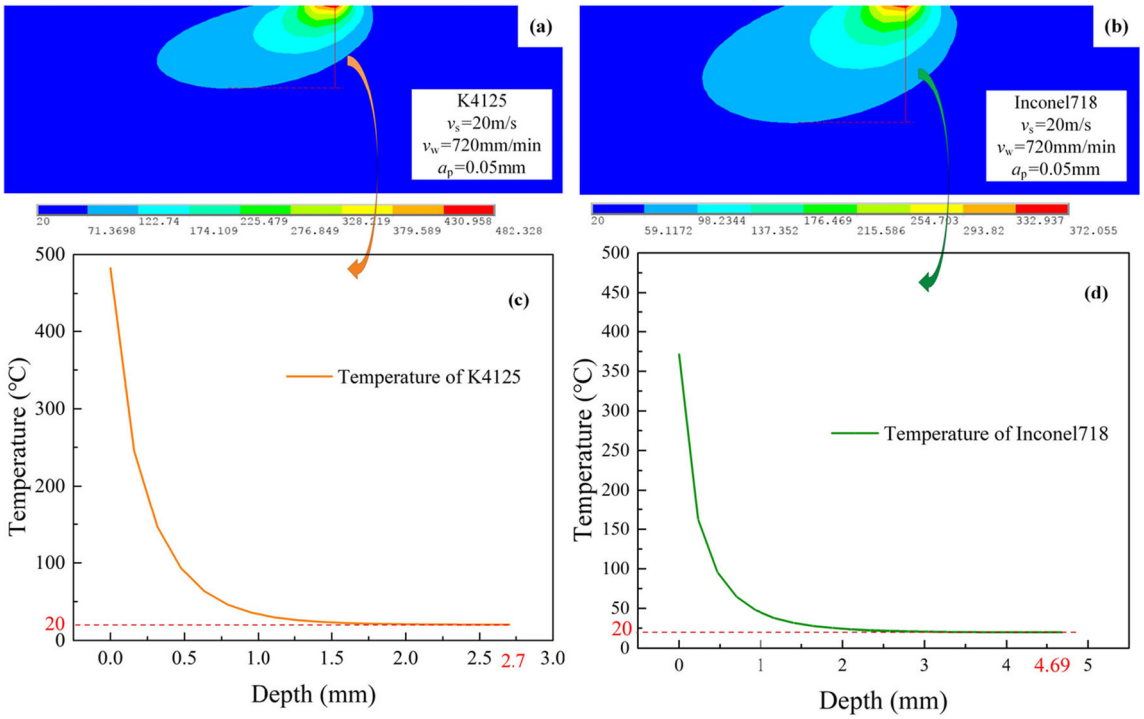

Fig. 6 Simulated thermal fields of K4125 and Inconel718 at the grinding speed of 20 m/s: **a** thermal field of K4125, **b** thermal field of Inconel718, **c** temperature curve along the depth of K4125, and **d** temperature curve along the depth of Inconel718

loading of the abrasive wheel. When the depth of cut rises from 0.01 to 0.1 mm, the grinding temperature of K4125 and Inconel718 rapidly increase, as shown in Fig. 5c. This is because the deeper depth of cut, on one hand, enlarges the a_{gmax} and increases the grinding force, which generates more heat, and, on the other hand, makes the heat difficult to dissipate. From the aspect of grinding temperature, the temperature of K4125 changes differently from Inconel718 because of the competition between the more friction, elastic and plastic deformation energy caused by the thinner a_{gmax} and more heat brought out by chips and cooling fluid. For example, in regard to Inconel718, the a_{gmax} descents with the increase of grinding speed; therefore, more heat is transferred into chips and then brought out; the cooling fluid is also easier to enter the grinding zone, then improves the cooling and lubricant. As a result, the grinding temperature of Inconel718 decreases. On the contrary, since the thermal conductivity of K4125 is lower, the heat brought out by the thinner chips and the effect of cooling fluid is limited. Besides, as mentioned above, the thinner a_{gmax} leads to more sliding and plowing which produce more heat. Thereby, the grinding temperature of K4125 enhances along with the grinding speed.

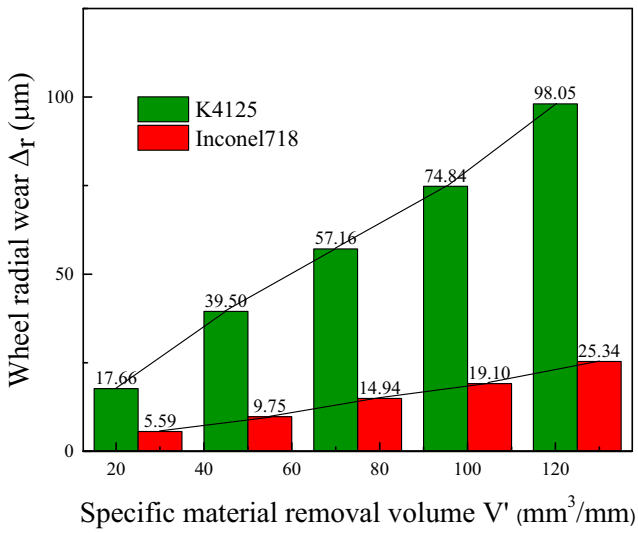

Fig. 7 Wheel radial wear trend

In addition, the thermal conductivity of K4125 is 13.2 W/m K, which is lower than that of Inconel718, i.e., 17.8 W/m K. Due to this fact, the proportion of heat transferring to workpiece R_w of K4125 is smaller; as a result, the heat gathers on the surface and the grinding temperature consequently is high. The mentioned proportion R_w can be derived by the combination of theoretical computation and experimental measurement. Based on the two-dimensional heat transfer models of oblique moving heat source with uniform heat flux [33], the proportion of heat transferring to workpiece R_w can be calculated as:

$$R_w = \frac{2A\pi\kappa}{F_t v_s \theta} e^{\frac{x'^2+z'^2}{2\alpha}} K_0^{-1}\left(\frac{v\sqrt{x'^2+z'^2}}{2\alpha}\right), K_0(u) = \frac{1}{2}\int_0^{\infty}\frac{d\omega}{\omega} e^{-\omega-\frac{u^2}{4\omega}} \quad (5)$$

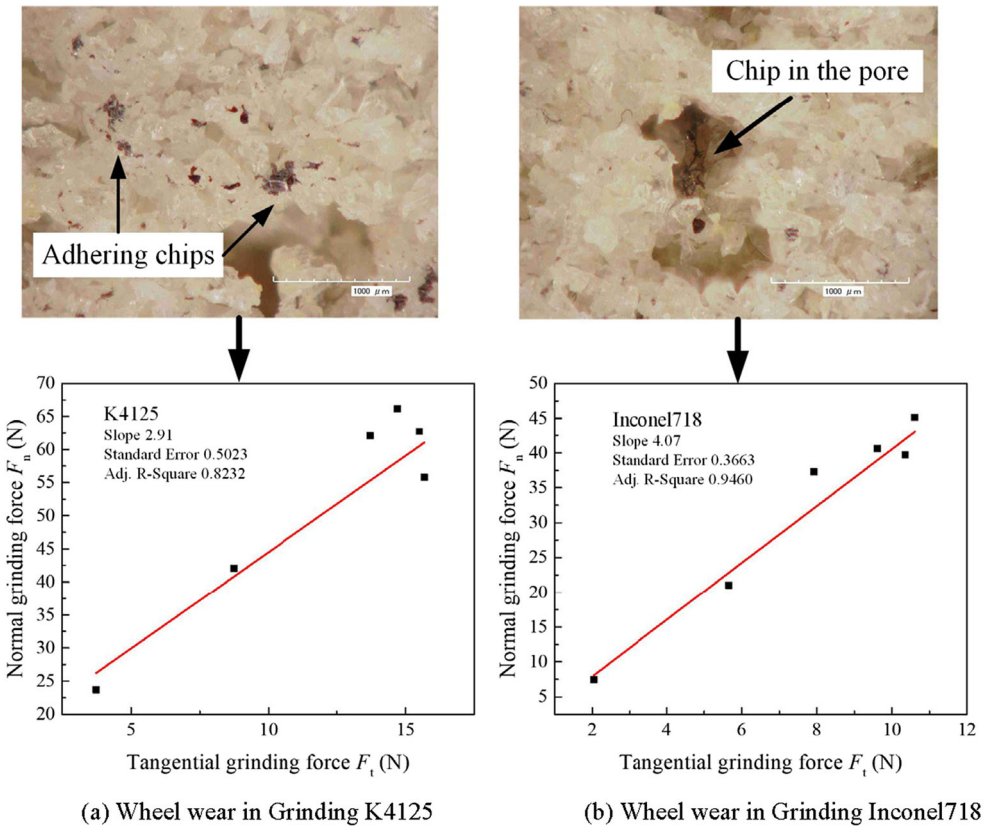

Fig. 8 Worn wheel surfaces and fittings of linear relation between normal and tangential forces of **a** K4125 and **b** Inconel718

where A is the contact area between the heat source and workpiece and α and κ are the diffusivity and thermal conductivity of the material. The proportion R_w of K4125 and Inconel718 can be computed according to Eq. 5, and it is shown in Table 4 that the R_w of K4125 is much lower than that of Inconel718.

The thermal fields of grinding K4125 and Inconel718 at grinding speed of 15, 20, 25, and 30 m/s are acquired by ANSYS software. The results are listed in Table 5. The graphs of thermal fields and temperature curves at different depth under the grinding speed of 20 m/s are shown in Fig. 6. It is clear that due to the lower thermal conductivity and smaller R_w of K4125, the heat is gathered around the ground surface, relatively the temperature gradient of K4125 is higher. Moreover, the depth of thermal field of K4125 ground surface is much smaller than that of Inconel718, almost half of that of Inconel718, e.g., as shown in Table 5 and Fig. 6; at the grinding speed of 20 m/s, the depth of thermal field of K4125 is 2.69 mm, whereas the Inconel718's is 4.69 mm.

In general, as demonstrated in Figs. 5 and 6, due to the mechanical property, the R_w of K4125 is smaller than the R_w of Inconel718; hence the grinding heat of K4125 is easy to gather around the ground surface and the thermal field depth of K4125 is shallower. Consequently, the temperature generated by the grinding K4125 process is evidently higher than the temperature from the grinding Inconel718 process.

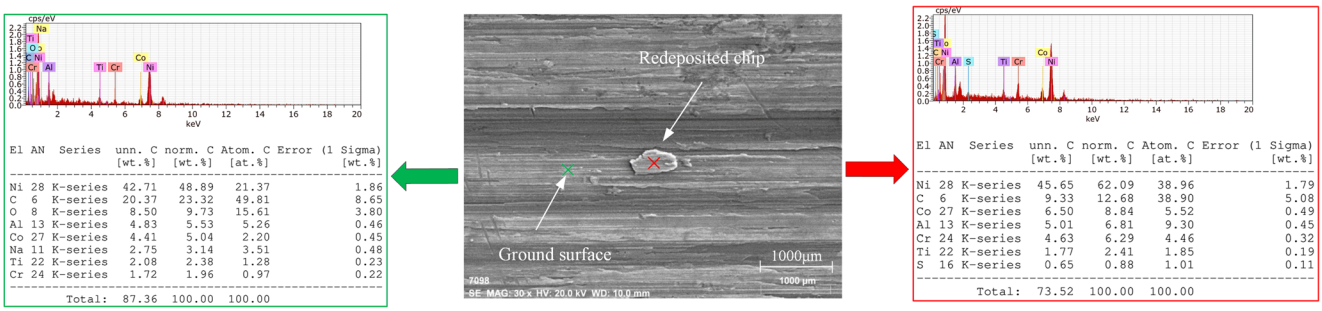

Fig. 9 The energy spectrum and element contents of ground surface and redeposited chip of K4125

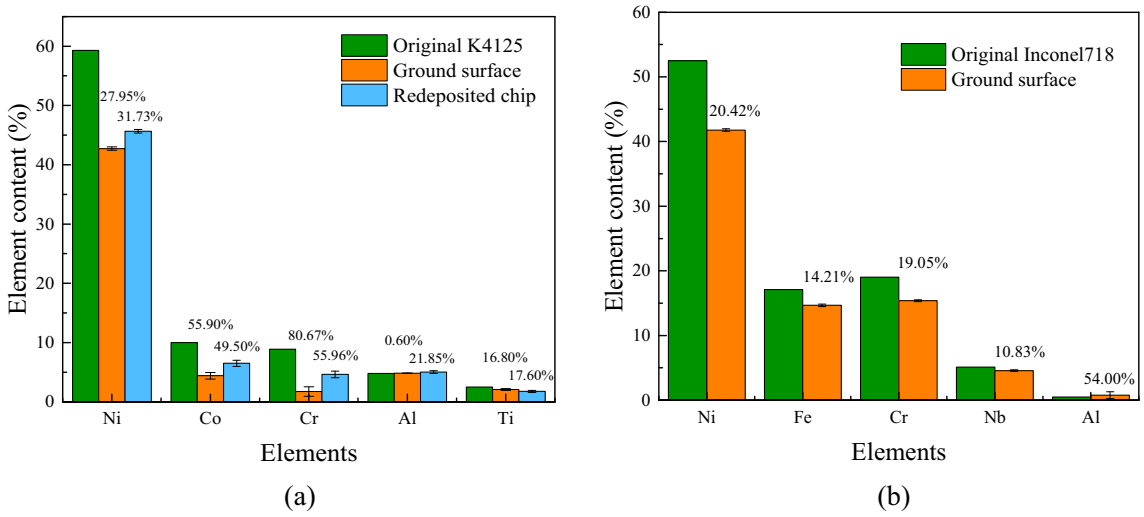

Fig. 10 Element content analysis of **a** K4125 and **b** Inconel718

3.3 Wheel wear analysis

When grinding nickel-based superalloy, the severe wheel wear can take places and further deteriorates the grinding performance [34, 35]. The worn wheel surface was copied by grinding graphite. Then, the cross-sectional surface of the graphite was observed to measure the radial wear of the wheel Δ_r. Figure 7 shows the wheel radial wear Δ_r against the specific material removal volume V'. The wheel radial wear Δ_r increases almost linearly along with the specific material removal volume. When grinding K4125, the wheel radial wear is raised from 17.66 to 98.05 μm. For Inconel718, the wheel radial wear increases from 5.59 to 25.34 μm, along with the material removal volume. The increasing trend of radial wear of grinding K4125 is greater than that of grinding Inconel718. The slope of radial wear line of grinding K4125 in Fig. 7 is 0.80, which is four times of the slope of radial wear line of grinding Inconel718, i.e., 0.20. This is clearly demonstrated that the wheel is easier to wear when grinding K4125; in turn, the lifetime is shorter.

Figure 8 illustrates the phenomenon of chip adhering on the wheel surface when grinding K4125 and Inconel718. It is more severe for K4125 chips to stick to the wheel than Inconel718 chips. The proportion of the chips adhering to the wheel A_{ad} is defined as the area of chip adhesion over the wheel surface area, and it was measured in this experiment. When $V' = 25$ mm^3/mm, the A_{ad} of K4125 is 0.34%; nonetheless, the A_{ad} of Inconel718 is 0.11%.

In addition, it is an interesting phenomenon that the chips of K4125 have a strong inclination to adhere to the grinding wheel, while the chip adhesion is not noticeable for Inconel718. The element contents were captured through the energy spectrum, as shown in Fig. 9. The element content analysis of original workpiece material, ground surface, and the redeposited chip is illustrated in Fig. 10a. The Al content of ground surface hardly changes. While due to the adhesion, some Al transferred from corundum grain into the chip and the content in the redeposited chips increases slightly. Thereby, the Al element has a limited contribution to the chip adhesion. The top 5 elements by contents in K4125 are Ni, Co, Cr, Al, and Ti. After grinding, the Ni, Co, and Cr element contents drop dramatically by 27.95, 55.90, and 80.67% respectively (as shown in Fig. 10a); this might explain the chip adhesion phenomenon. The deposited chip, which firstly stuck to the grain and then redeposited on the ground surface, is further analyzed, and the element changes bear a resemblance with the ground surface. Since the oxides of Cobalt (Co_2O_3) and Chrome (Cr_2O_3) have similar lattice structure parameters with

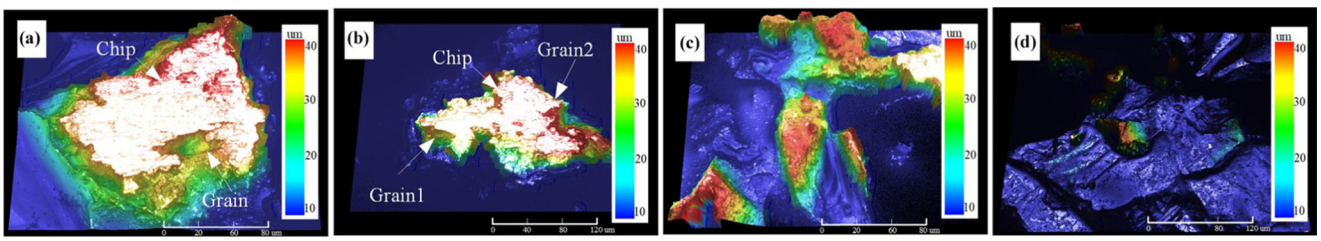

Fig. 11 Morphology of grains after grinding: **a** grain with adhesion chip, **b** two grains covered by a chip, **c** blunt grain with fracture, **d** sharp grain (v_s=30 m/s, v_w=720 mm/min, a_p=0.05 mm, two grinding passes)

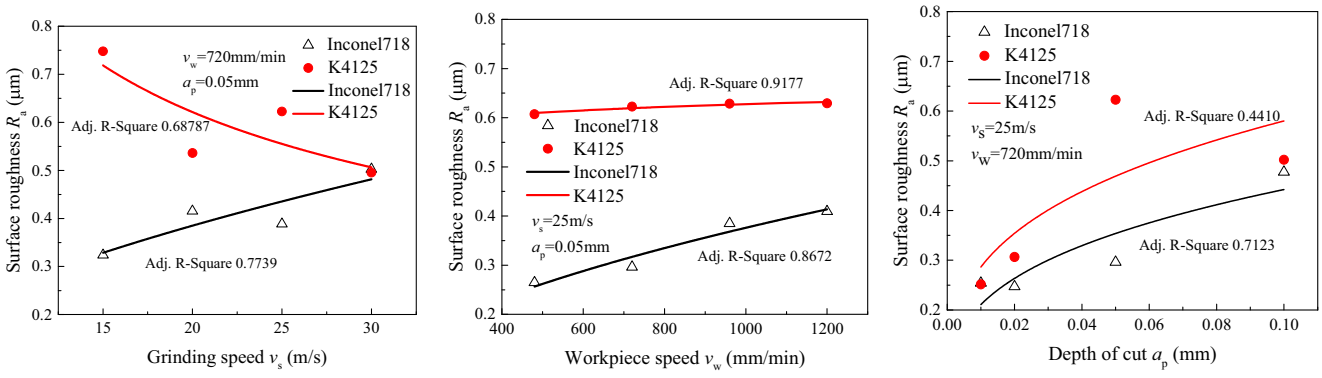

Fig. 12 Effects of **a** grinding speed, **b** workpiece speed and **c** depth of cut on ground surface roughness

the corundum, when the chips contact with the grains, the Co, Cr, and Ni elements transfer into the grains, take the place of Al, and have strong covalent bonds with O element. As a result, the chips are easy to attach to the grains. As for Inconel718, however, the element content analysis shows that the element transference of Ni, Fe, Cr, and Nb is lower than K4125. Relatively, the contents of Ni, Fe, Cr, and Nb drop by 20.42, 14.21, 19.05, and 10.83% respectively (as shown in Fig. 10b). Accordingly, the lower element exchange and interaction lead to little chip adhesion for Inconel718.

Correspondingly, due to chip adhesion, there are four typical types of grain morphology when grinding K4125, i.e., grains with adhering chips (Fig. 11a), several grains covered by adhering chips (Fig. 11b), blunt grain with attrition or fracture (Fig. 11c), and sharp grains (Fig. 11d). Whereas the grain condition is much better when grinding Inconel718, which consists of sharp grains (Fig. 11d), grains with attrition (similar with the grain shown in Fig. 11a) and the effect of chip adhesion can be neglected.

3.4 Ground surface roughness analysis

The ground surface roughness is also an important index of the grinding performance, since the fatigue lifetime of the part strongly depends on surface roughness [36–38]. Therefore, it is necessary to investigate the influence of the grinding

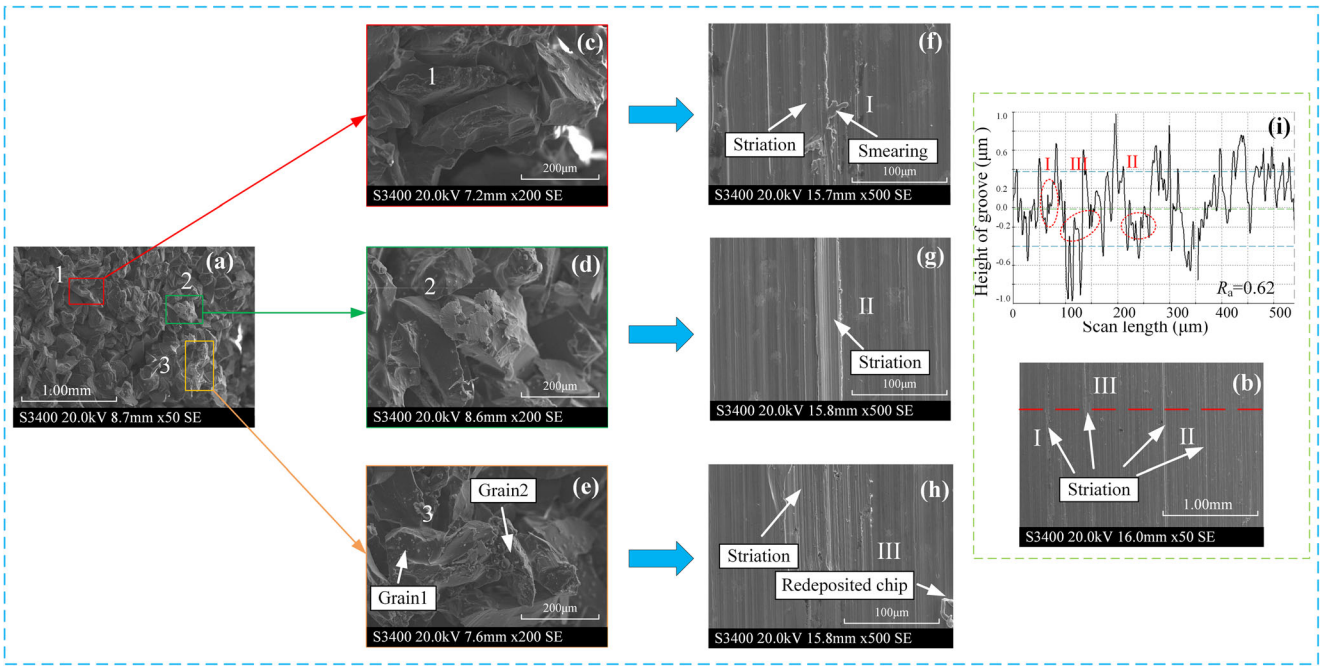

Fig. 13 Surface generation of grinding K4125: **a** SEM graph of the wheel surface, **b** SEM graph of the ground surface, **c** SEM graph of the fracture grain, **d** SEM graph of the grain with a adhering chip, **e** SEM graph of the joint grains, **f** SEM graph of the ground surface zone I, **g** SEM graph of the ground surface zone II, **h** SEM graph of the ground surface zone III, and **i** the section profile of the ground surface

parameters on the ground surface roughness. The influence of grinding parameters on the surface roughness is illustrated in Fig. 12. As mentioned above, with the rise of the grinding speed, the temperature in the grinding zone rises, the plasticity of Inconel718 is raised, and the material removal ability of grains decreases. Consequently, the side-flows and pile-ups increase and then worsen the surface. As for K4125, the better thermal strength constrains the side-flows and pile-ups; furthermore, the smaller a_{gmax} reduces the residual materials on the surface [39–41]. Accordingly, the surface roughness of K4125 improves from 0.75 to 0.50 μm along with the increase of the grinding speed. When the workpiece speed increases, the surface roughness of K4125 stays stable around 0.6 μm. On the contrast, the surface roughness of Inconel718 is deteriorated from 0.27 to 0.41 μm. When the depth of cut rises, the surface roughness of K4125 and Inconel718 increase respectively. This is attributed to the change of a_{gmax}. For the Inconel718, it is easy to obtain the R_a 0.4 μm surface by grinding. However, it is challenging for K4125 to obtain the R_a 0.4 μm surface.

3.5 Ground surface topography analysis

Figures 13 and 14 are the demonstrations of the ground surface generation of K4125 and Inconel718. From the SEM graphs of the ground surfaces in Figs. 13b and 14b, it is illustrated that the surface quality of K4125 is worse than that of Inconel718. The ground surface of K4125 consists of some defects, such as wide and deep striations, smearing, redeposited chips, as shown in Fig. 13f–h, whereas the ground surface of Inconel718 is formed by tiny grinding tracks with few defects as shown in Fig. 14. The ground surface quality heavily depends on the grain conditions [42], which are shown in Figs. 11 and 13. The blunt grains with attrition or fracture (Figs. 11c and 13c) have weaker material removal ability and, therefore, can cause some side-flows, pile-ups, and smearing along the grinding tracks (Fig. 13f). The adhering chips cover the cutting edges of grains, then make the grains wider and higher (Figs. 11a and 13d). Specially, some chips fill in the pores between grains and joint several cutting edges together (Figs. 11b and 13e) make the joint cutting edge more than 150 μm wide. This deteriorates the sharpness of the grains, harms the grains' protrusion height distribution, and further leads to deep and enlarged striations on the ground surface (Fig. 13g, h). More specifically, in Fig. 13i, the profile of ground surface, the groove I is caused by a blunt grain, while the groove II is formed by the grain with an adhering chip and the groove III is generated by joint grains. In addition, the adhering chips blunt the grains and increase the

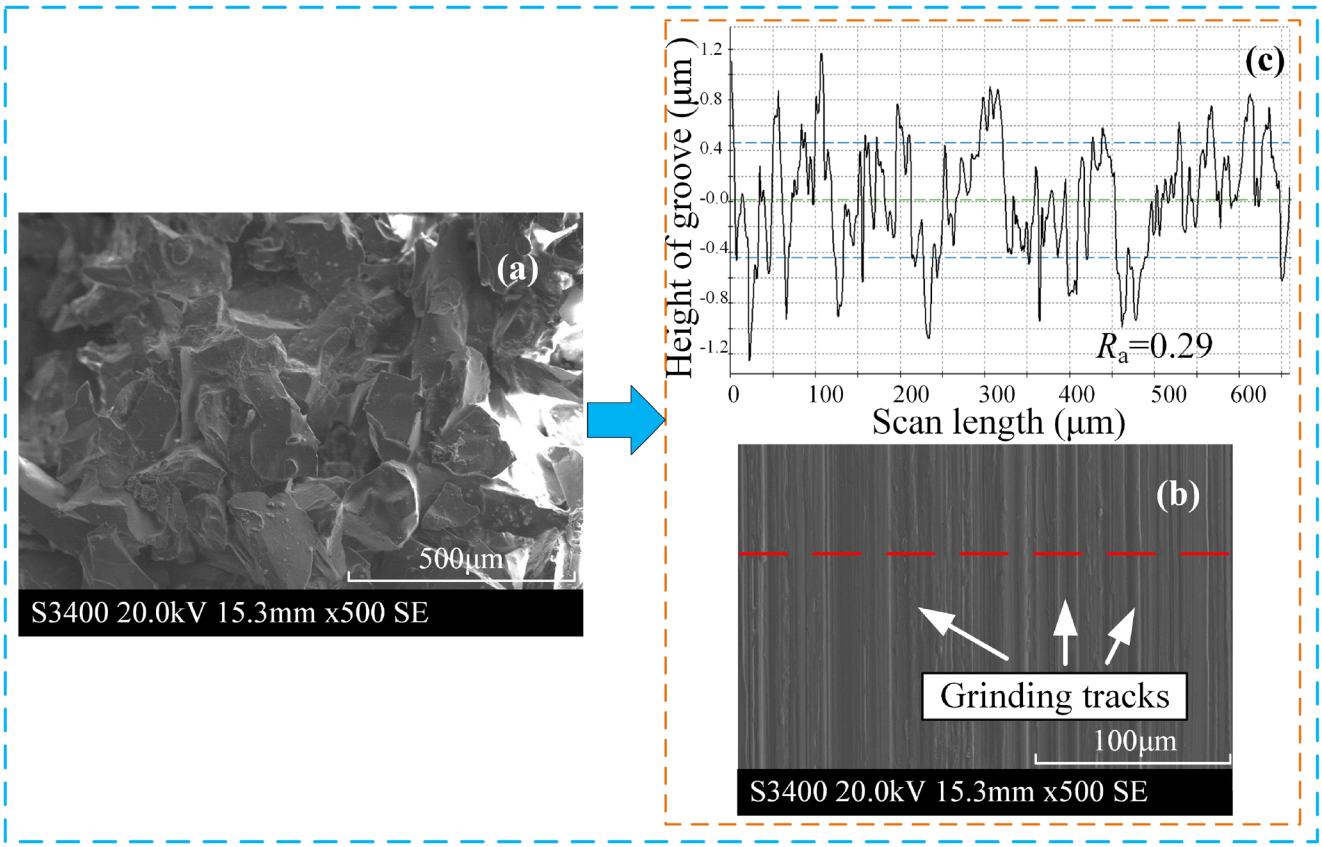

Fig. 14 Surface generation of grinding Inconel718: **a** SEM graph of the wheel surface, **b** SEM graph of the ground surface, and **c** the sectional profile of the ground surface

friction between the grain and workpiece, therefore bringing about more plowing and plastic flows on the surface. As for grinding Inconel718, most grains are sharp (Fig. 14a), and chips are stored in the pores instead of sticking to the wheel surface, so the ground surface is formed by tiny grinding tracks with a few defects, as shown in Fig. 14b. Consequently, the smearing, side-flows, and pile-ups on the K4125 ground surface are more than the ground surface of Inconel718. It is more challenging to grind a fine surface of K4125 than Inconel718.

4 Conclusion

In this paper, the comparative experiments of grinding equiaxed cast nickel-based superalloy K4125 and wrought nickel-based superalloy Inconel718 are conducted by the brown corundum wheel. The influence of grinding parameters (i.e., grinding speed, workpiece speed, and depth of cut) on the grinding force, specific grinding energy, wheel wear, and ground surface quality is investigated. Some findings are obtained as follows:

(1) Because of the better mechanical property of K4125 than Inconel718 and a strong affinity between the K4125 and the corundum wheel, it is more difficult to grind K4125. Therefore, the grinding force and specific grinding energy of K4125 are always larger than those of Inconel718 regardless of the grinding parameters in this experiment.
(2) Due to the lower thermal conductivity, the R_w value of K4125 is smaller than that of Inconel718; hence, the grinding heat of K4125 is much easier to gather around the ground surface, and the thermal field depth of K4125 is shallower. Consequently, the grinding temperature of K4125 is evidently higher than that of Inconel718, e.g., the temperature from the grinding K4125 process is above 400 °C and, as for grinding Inconel718 process, the temperature is below 200 °C under the present experimental conditions.
(3) Because of the exchange of Co and Cr elements between the workpiece and grains, the chips are easier to adhere on the wheel surface when grinding K4125, the proportion of chip adhering area of K4125 is three times of that of Inconel718. When grinding K4125, the grains are in four conditions, i.e., grains with chips, several grains jointed by chips, grains with attritions or fractures and sharp grains. As a result, the wheel wear of grinding K4125 is severe and the lifetime is shorter.
(4) The defects such as smearing, redeposited chips, and striations on the ground surface of K4125 are more than those on the ground surface of Inconel718. Besides, the surface roughness of K4125 is higher than that of Inconel718. Thereby, it is more challenging to obtain a fine ground surface of K4125.

Acknowledgements The authors gratefully acknowledge the financial support for this work by the National Natural Science Foundation of China (No. 51775275 and No. 51705463) and the Fundamental Research Funds for the Central Universities (No. NE2014103 and No. NZ2016107).

References

1. Tso PL (1995) Studying on the grinding of Inconel718. J Mater Process Technol 55:421–426
2. Gift FC, Misiolek WZ, Force E (2004) Fluid performance study for groove grinding a nickel-based superalloy using electroplated cubic boron nitride (CBN) grinding wheels. J Manuf Sci Eng Trans ASME 126(8):451–458
3. Caruso S, Imbrogno S, Rotella G, Ciaran MI, Arrazola PJ, Filice L, Umbrello D (2015) Numerical simulation of surface modification during machining of nickel-based superalloy. Procedia CIRP 31: 130–135
4. Chen M, Li XT, Sun FH, Xiang Y, Xue B (2001) Studies on the grinding characteristics of dictionally solidified nickel-based superalloy. J Mater Process Technol 116:165–169
5. Gift FC, Misiolek WZ, Force E (2004) Mechanics of loading for electroplated cubic boron nitride (CBN) wheels during grinding of a nickel based superalloy in water-based lubricating fluids. J Tribol Trans ASME 126(4):795–801
6. Upadhyaya RP, Malkin S (2004) Thermal aspects of grinding with electroplated CBN wheels. J Manuf Sci Eng Trans ASME 126(2): 107–114
7. Klocke F, Soo SL, Karpuschewski B, Webster JA, Novovic D, Elfizy A, Axinte DA, Tönissen S (2015) Abrasive machining of advanced aerospace alloys and composites. CIRP Ann Manuf Technol 64:581–604
8. Xi XX, Ding WF, Fu YC, Xu JH (2018) Grindability evaluation and tool wear during grinding of Ti_2AlNb intermetallics. Int J Adv Manuf Technol 94:1441–1450
9. Österle W, Li PX (1997) Mechanical and thermal response of a nickel-base superalloy upon grinding with high removal rates. Mater Sci Eng A 238(2):357–366
10. Öpöz TT, Chen X (2015) Experimental study on single grit grinding of Inconel 718. Proc Inst Mech Eng B J Eng Manuf 229(5):713–726
11. Tian L, Fu Y, Xu J, Li HY, Ding WF (2015) The influence of speed on material removal mechanism in high speed grinding with single grit. Int J Mach Tools Manuf 89:192–201
12. Dai JB, Ding WF, Zhang LC, Xu JH, Su HH (2015) Understanding the effects of grinding speed and undeformed chip thickness on the chip formation in high-speed grinding. Int J Adv Manuf Technol 81(5–8):995–1005
13. Dai CW, Ding WF, Xu JH, Fu YC, Yu TY (2017) Influence of grain wear on material removal behavior during grinding nickel-based superalloy with a single diamond grain. Int J Mach Tools Manuf 113:49–58
14. Liu Q, Chen X, Gindy N (2007) Assessment of Al_2O_3 and superabrasive wheels in nickel-based alloy grinding. Int J Adv Manuf Technol 33:940–951

15. Chen ZZ, Xu JH, Ding WF, Ma CY, Fu YC (2015) Grinding temperature during high-efficiency grinding Inconel718 using porous CBN wheel with multilayer defined grain distribution. Int J Adv Manuf Technol 77:165–172
16. Li QL, Xu JH, Su HH, Lei W (2015) Fabrication and performance of monolayer brazed CBN wheel for high-speed grinding of superalloy. Int J Adv Manuf Technol 80:1173–1180
17. Zhong ZW, Ramesh K, Yeo SH (2001) Grinding of nickel-based super-alloys and advanced ceramics. Mater Manuf Process 16(2): 195–207
18. Xu XP, Yu YQ, Xu HJ (2002) Effect of grinding temperatures on the surface integrity of a nickel-based superalloy. J Mater Process Technol 129:359–363
19. Ding WF, Xu JH, Chen ZZ, Su HH, Fu YC (2010) Grindability and surface integrity of cast nickel-based superalloy in creep feed grinding with brazed CBN abrasive wheels. Chin J Aeronaut 23(4):501–510
20. Ding WF, Xu JH, Chen ZZ, Su HH, Fu YC (2010) Wear behavior and mechanism of single-layer brazed CBN abrasive wheels during creep-feed grinding cast nickel-based superalloy. Int J Adv Manuf Technol 51:541–550
21. Spur G, Niewelt W (1994) Creep feed grinding of Nickel-based alloys with advanced corundum and with CBN-grinding wheels. 7th International Conference on Production/Precision Engineering, Chiba, Japan, 15–17 September 1994
22. Zhao ZC, Xu JH, Fu YC, Zhang ZW (2013) Creep feed grinding of Ni-based superalloy with micro-crystalline ceramic alumina wheels. Adv Mater Res 797:511–515
23. Sinha MK, Setti D, Ghosh S, Rao PV (2016) An investigation on surface burn during grinding of Inconel718. J Manuf Process 21: 124–133
24. Yang M, Li CH, Zhang YB, Jia DZ, Hou ZXP, Y L LIRZ, Wang J (2017) Maximum undeformed equivalent chip thickness for ductile-brittle transition of zirconia ceramics under different lubrication conditions. Int J Mach Tools Manuf 122:55–65
25. Zhang YB, Li CH, Ji HJ, Yang XH, Yang M, Jia DZ, Zhang XP, Li RZ, Wang J (2017) Analysis of grinding mechanics and improved predictive force model based on material-removal and plastic-stacking mechanisms. Int J Mach Tools Manuf 122:81–97
26. Zhang ZY, Cui JF, Wang B, Wang ZG, Kang RK, Guo DM (2017) A novel approach of mechanical chemical grinding. J Alloys Compd 726:514–524
27. Heinzel C, Bleil N, Peters J (2007) The use of the size effect in grinding for work-hardening. CIRP Ann Manuf Technol 56(1): 327–330
28. Ghosh S, Chattopadhyay AB, Paul S (2008) Modelling of specific energy requirement during high-efficiency deep grinding. Int J Mach Tools Manuf 48(11):1242–1253
29. Rowe WB, Chen X (1997) Characterization of the size effect in grinding and the sliced bread analogy. Int J Prod Res 35(3):887–899
30. Yang SB, Xu J, Fu Y, Wei WH (2012) Finite element modeling of machining of hydrogenated Ti-6Al-4V alloy. Int J Adv Manuf Technol 59:253–261
31. Chen J, Shi DQ, Miao GL, Yang XG (2017) Effect of maximum temperature on the thermal fatigue behavior of superalloy GH536. Appl Mech Mater 853:28–32
32. Zhang ZY, Shi ZF, Du YF, Yu ZJ, Guo LC, Guo DM (2018) A novel approach of chemical mechanical polishing for a titanium alloy using an environment-friendly slurry. Appl Surf Sci 427: 409–415
33. Jin T, Cai GQ (2001) Analytical thermal models of oblique moving heat source for deep grinding and cutting. J Manuf Sci Eng Trans ASME 123(2):185–190
34. Yu TY, Bastawros AF, Chandra A (2017) Experimental and modeling characterization of wear and life expectancy of electroplated CBN grinding wheels. Int J Mach Tool Manu 121:70–80
35. Zhang ZY, Huang SL, Wang SC, Wang B, Bai Q, Zhang B, Kang RK, Guo DM (2017) A novel approach of high-performance grinding using developed diamond wheels. Int J Adv Manuf Technol 91: 3315–3326
36. Zhou HX, Guo M, Wang XZ (2017) Ultraprecision grinding of silicon wafers using a newly developed diamond wheel. Mater Sci Semicond Process 68:238–244
37. Mao C, Zhou X, Lin LR, Zhang MJ, Tang K, Zhang J (2016) Investigation of the flow field for a double-outlet nozzle during minimum quantity lubrication grinding. Int J Adv Manuf Technol 85:291–298
38. Yao CF, Tan L, Yang P, Zhang DH (2018) Effects of tool orientation and surface curvature on surface integrity in ball end milling of TC17. Int J Adv Manuf Technol 94:1699–1710
39. Butler-Smith P, Axinte D, Daine M, Kong MC (2014) Mechanisms of surface response to overlapped abrasive grits of controlled shapes and positions: an analysis of ductile and brittle materials. CIRP Ann Manuf Technol 63(1):321–324
40. Chen C, Tang JY, Chen HF, Zhou CC (2017) Research about modeling of grinding workpiece surface topography based on real topography of grinding wheel. Int J Adv Manuf Technol 93:2411–2421
41. Jia DZ, Li CH, Zhang YB, Yang M, Wang YG, Guo SM, Cao HJ (2017) Specific energy and surface roughness of minimum quantity lubrication grinding Ni-based alloy with mixed vegetable oil-based nanofluids. Precis Eng 50:248–262
42. Zhang MJ, Tan Y, Zhou FJ, Mao C, Xie ZZ, Li CH (2017) Analysis of flow field in cutting zone for spiral orderly distributed fiber tool. Int J Adv Manuf Technol 92:4345–4354